

Constructing bifunctional and robust covalent organic frameworks via three-component one-pot Doebner reaction for Cr(VI) removal

Muzammil Hussain^a, Anam Saddique^a, Kamakshaiah Charyulu Devarayapalli^b, Bolam Kim^b, In Woo Cheong^a, Dae Sung Lee^{b,*}

^a Department of Applied Chemistry, Kyungpook National University, 80 Daehak-ro, Buk-gu, Daegu 41566, Republic of Korea

^b Department of Environmental Engineering, Kyungpook National University, 80 Daehak-ro, Buk-gu, Daegu 41566, Republic of Korea

ARTICLE INFO

Keywords:

Covalent organic framework
Doebner reaction
Linkage functionalization
Cr(VI) removal
Adsorption and photocatalytic reduction synergy

ABSTRACT

The integral part of covalent organic frameworks (COFs) is covalent bonds. Thus, stable and functional links must be developed to expand the potential applications of COFs. Herein, in situ linkage functionalization using a three-component irreversible Doebner reaction was achieved to fabricate chemically stable carboxylic acid-bearing COFs (Tp-Tta-COOH and Tp-Tapb-COOH), which have abundant chelating groups and ordered electron donor-acceptor moieties facilitating charge separation for effective Cr(VI) adsorption and photoreduction, respectively. These functionalized COFs are more effective at Cr(VI) removal via adsorption and photoreduction than their unfunctionalized counterparts (Tp-Tta and Tp-Tapb). The synergy of adsorption and photocatalysis is crucial to effectively remove Cr(VI) from aqueous solutions. This synergy empowers Tp-Tta-COOH to be used continuously for Cr(VI) removal without any elution after each cycle. Furthermore, Tp-Tta-COOH exhibits high chemical stability, durability, and recyclability. This study will promote the development of durable and useful COF materials for real-world applications.

1. Introduction

Covalent organic frameworks (COFs) are porous, crystalline organic polymeric materials held together by covalent bonds between their constituent organic building components [1]. At present, most efforts on the construction of functional β -ketoenamine-linked COFs have focused on the design and management of organic building units. The condensation of the aldehyde building block triformylphloroglucinol (Tp) with amine monomers bearing the corresponding functional groups resulted in the introduction of COOH, OH, NO₂, OCH₃, CF₃, SO₃H, and F into the β -ketoenamine-linked framework [2–8]. However, the effect of linkage functionalization on COF characteristics and functions must not be overlooked. Exploring the linkage functionalization of COFs, particularly imine-linked COFs, has become a popular area of study. Given its chemical activity, the imine bond can be transformed into imidazole [9], thiazole [10], oxazole [11], and quinolines [12,13], which can provide COFs various exciting properties, such as excellent chemical stability and improved light harvesting. However, most linkage functionalization reports are limited to imine-linked COFs, which significantly reduces the diversity of COFs. Hence, creating a synthetic approach for

functionalizing β -ketoenamine-linked COFs is favorable to improve their characteristics.

Hexavalent chromium (Cr(VI)), which is used extensively in the chemical, electronic, and printing industries, results in a substantial volume of Cr(VI)-comprising effluents [14,15]. This effluent must be treated to remove Cr(VI), which has been linked to several illnesses, for example, cancer [16]. Ultrafiltration [17], reduction and precipitation [18], adsorption [19], ion exchange [20], and photocatalysis [21] are a few of the technologies that have been applied to remove Cr(VI). Two of these technologies, adsorption and photocatalytic reduction, are effective and benign to the environment. COFs are novel polymer materials characterized by their exceptional stability, tunability, and porous structure and have been used effectively for water decontamination [22–24]. Given their π -conjugated highly ordered structures, COFs exhibit semiconducting properties, and they can be utilized for Cr(VI) photoreduction [25,26]. However, their effectiveness is limited because of the limited interaction with chromium species and rapid recombination of photoinduced electrons and holes. On the contrary, Cr(VI) adsorption was achieved by grafting different functional groups onto the COF molecular framework [14,19,27]. Nevertheless, COF adsorbents

* Corresponding author.

E-mail address: daesung@knu.ac.kr (D.S. Lee).

<https://doi.org/10.1016/j.apcatb.2023.123672>

Received 29 August 2023; Received in revised form 1 December 2023; Accepted 27 December 2023

Available online 29 December 2023

0926-3373/© 2023 Elsevier B.V. All rights reserved.

must be regenerated after each adsorption cycle by immersing in an acid or alkaline solution. We set out to proceed with a hybrid approach that combines adsorption and photocatalytic techniques to remove Cr(VI) from water more effectively than either technique could do alone.

In this study, two novel, robust, porous, crystalline, and bifunctional carboxylic acid-decorated β -ketoenamine-linked COFs (Tp-Tta-COOH and Tp-Tapb-COOH) was rationally designed and fabricated via linkage functionalization using a three-component (aldehyde, amine, and pyruvic acid (PA)) one-pot (OP) Doebner reaction. We have expanded the application of the three-component OP approach for linkage functionalization via the Doebner reaction to β -ketoenamine-linked COFs, which were initially limited to imine-linked COFs. Moreover, to evaluate the impact of linkage functionalization on structural properties and Cr(VI) removal ability, the corresponding nonfunctionalized β -ketoenamine-linked COFs (Tp-Tta and Tp-Tapb) were also constructed (Fig. 1A). Linkage functionalization can effectively tune COF properties. Consequently, functionalized COFs outperform their unfunctionalized counterparts with regard to the adsorption and photoreduction of Cr(VI) due

to the inclusion of carboxylic acid-chelating groups, narrow band gap, enhanced light harvesting ability, improved electron-hole pair generation, and separation efficiency. To the best of our knowledge, this type of functionalization is the first of its kind in β -ketoenamine-linked COFs.

2. Materials and methods

2.1. Synthesis of COFs

2.1.1. Preparation of Tp-Tta-COOH

Tp (0.083 mmol, 17.44 mg) and 4,4',4''-(1,3,5-Triazine-2,4,6-triyl) trianiline (Tta)(0.083 mmol, 29.42 mg) were added in a 10-mL Biotage microwave vial. Afterward, 1,4-dioxane (0.60 mL), dimethyl sulfoxide (DMSO)(0.40 mL), *p*-toluenesulfonic acid monohydrate (TsOH)(2 mg), PA (0.023 mL), and acetic acid (0.03 mL) were added to the vial and sonicated for 30 min. Freeze-pump-thaw cycles were applied to the reaction mixture before being sealed in nitrogen atmosphere. Then, the vial was placed in a 120 °C oven and left undisturbed for a duration of 3

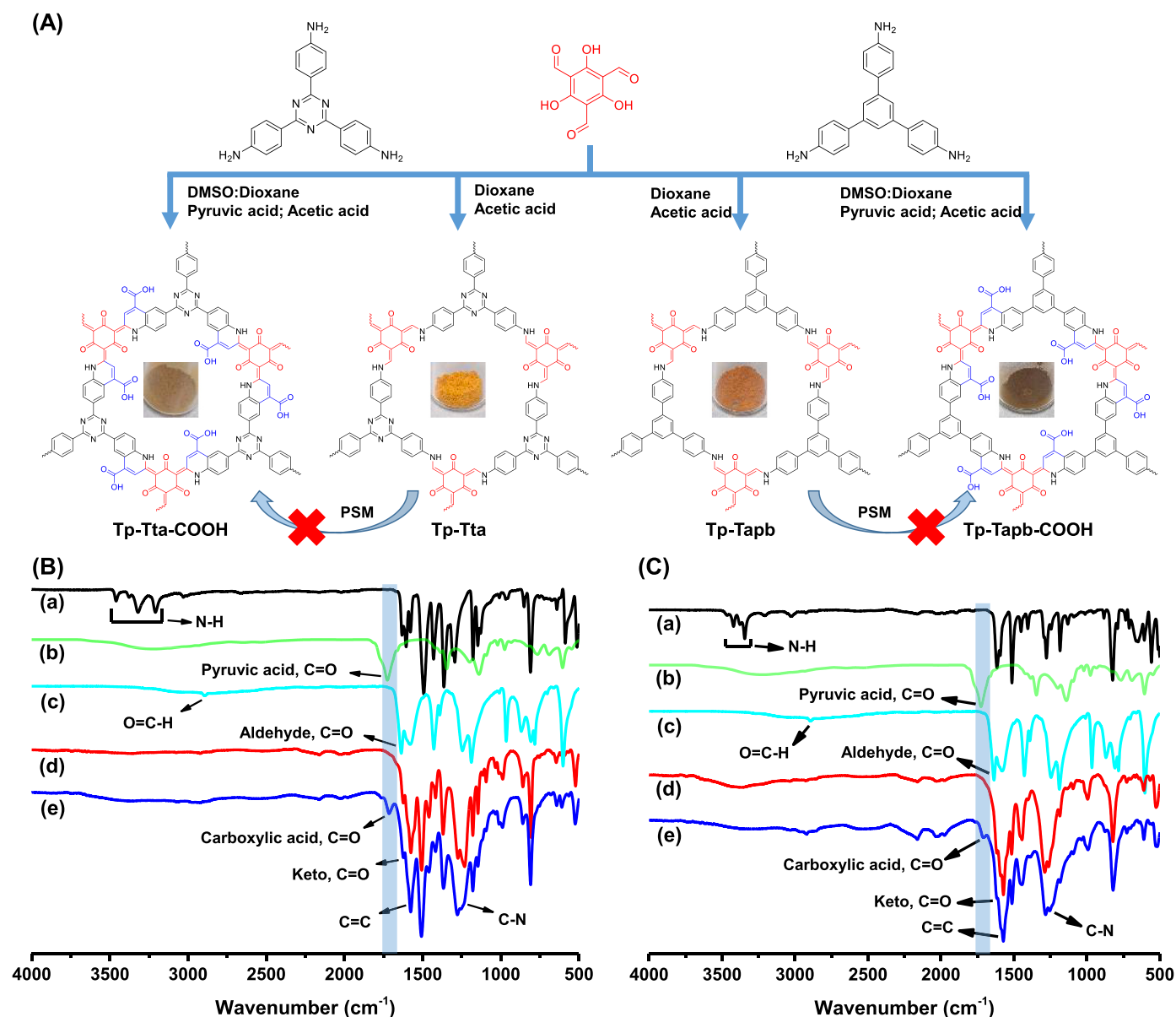


Fig. 1. Synthesis and characterization of synthesized COFs: (A) synthesis scheme for Tp-Tta, Tp-Tta-COOH, Tp-Tapb-COOH, and Tp-Tapb (corresponding photographs of the materials are shown in the inset). (B, C) FT-IR spectrum; (B), (a) Tta, (b) PA, (c) Tp, (d) Tp-Tta, and (e) Tp-Tta-COOH; (C), (a) Tapb, (b) PA, (c) Tp, (d) Tp-Tapb, and (e) Tp-Tapb-COOH.

days. After the vial was cooled, the extracted powder was vacuum-filtered and washed with dimethylformamide (DMF), water, and copious amount of ethanol and acetone. The powder was initially dried in a fume hood and then activated under vacuum conditions at a temperature of 90 °C for a duration of 6 h. Elemental analysis of $C_{39}H_{18}N_6O_9$ was performed as follows: C (65.55%), H (2.54%), N (11.76%); observed C (62.96%), H (3.78%), N (11.99%).

2.1.2. Preparation of Tp-Tabb-COOH

Tp-Tabb-COOH and Tp-Tta-COOH were synthesized in a similar manner by replacing the Tta monomer with the 1,3,5-Tris(4-amino-phenyl)benzene (Tapb) (0.083 mmol, 29.2 mg) monomer. Elemental analysis of $C_{42}H_{21}N_3O_9$ was performed as follows: C (70.89%), H (2.97%), N (5.90%); observed C (67.61%), H (4.43%), N (5.71%).

2.1.3. Preparation of Tp-Tta

Tp-Tta COF was synthesized using a modified version of a method found in published literature. Tp (0.083 mmol, 17.44 mg), Tta (0.083 mmol, 29.42 mg), 1,4-dioxane (1.0 mL), and 6 M acetic acid (0.1 mL) were added to a microwave vial (10 mL), and the vial was sonicated for 30 min. The reaction mixture underwent freeze-pump-thaw cycles, and then it was sealed off under nitrogen. The vial was kept undisturbed in an heating oven set at 120 °C for a duration of 3 days. The powder was collected after allowing the vial to cool, and it was vacuum filtered and washed with DMF, water, ethanol, and acetone. The powder underwent an initial drying process in a fume hood, and then activated under vacuum conditions at a temperature of 90 °C for 6 h. Elemental analysis of $C_{30}H_{18}N_6O_3$ was performed as follows: C (70.58%), H (3.55%), N (16.46%); observed C (64.09%), H (3.49%), N (14.25%).

2.1.4. Preparation of Tp-Tabb

Tp-Tabb and Tp-Tta were synthesized in a similar manner by replacing the Tta monomer with the Tapb (0.083 mmol, 29.2 mg) monomer. Elemental analysis of $C_{33}H_{21}N_3O_3$ was performed as follows: C (78.09%), H (4.17%), N (8.28%); observed C (74.28%), H (4.17%), N (7.40%).

2.2. Cr(VI) removal experiments

Experiments on the removal of Cr(VI) typically involve the dispersion of 5 mg of COF in 20 mL of Cr(VI) solution (50 ppm) at an initial pH of 1. Then, the reaction suspension was stirred using a magnetic stirrer in the dark for a duration of 60 min to reach adsorption equilibrium. Subsequently, the reaction suspension was exposed to ultraviolet (UV) light, which was generated by a medium-pressure mercury lamp with a power output of 100 W. The lamp was positioned in a quartz immersion well equipped with a water-circulating jacket to ensure a stable temperature of 25 °C. Alternatively, the suspension was subjected to simulated solar light produced by a 150 W Xenon (Xe) Arc lamp, part of the 10500 solar simulator manufactured by ABET Technologies. The experiment continued for an additional 120 min [28,29]. At predetermined time intervals, 1 mL of solution was collected, filtered through a 0.45- μ m PTFE syringe filter, and the supernatant was collected for diphenylcarbazide (DPC) colorimetry to measure the residual Cr(VI) content.

Further details regarding the materials, instruments, Cr(VI) removal and analysis parameters, photoelectrochemical measurements, quenching experiments, chemical stability, and cycle performance of Tp-Tta-COOH are given in [supplementary materials](#).

3. Results and discussion

The Doebner reaction was used for the functionalization of imine-linked COFs via post-synthetic modification (PSM) or OP [13]. However, the use of the Doebner reaction is limited to imine-linked COFs,

and its mechanism can be divided into two steps: formation of reversible imine bonds and irreversible cyclization of imine bonds with PA [12,30,31]. Thus, we extended the scope of the Doebner reaction to β -ketoenamine-linked COFs. The functionalization of β -ketoenamine-linked COFs using Doebner reaction is delicate as the construction mechanism of β -ketoenamine-linked COFs involves the formation of reversible imine bonds that are converted to irreversible β -ketoenamine linkages via keto-enol tautomerism. Once irreversible β -ketoenamine linkages developed in the framework, they cannot undergo cyclization with PA (Fig. S1). Therefore, the reaction parameters must be optimized to ensure the nucleophilic attack of PA on the imine bond before it undergoes keto-enol tautomerism. In addition, the proposed Doebner reaction mechanism for Tp-based COFs may be broken down into three steps: (1) imine bond formation via the Schiff base reaction, (2) PA-executed cyclization of the imine bond, and (3) tautomerism of enol to a keto form.

First, Tp, Tta, and PA were used to explore the feasibility of the OP three-component Doebner reaction for the formation of Tp-Tta-COOH COF. Initially, dioxane was used as a reaction solvent, which is the commonly used solvent for the fabrication of β -ketoenamine COFs, and the characteristic carboxylic acid carbonyl peak was not detected in the FT-IR spectrum [32]. The low activity of PA might be attributed to the low conversion rate of keto to an enol tautomeric form of PA, which is considered as an active species for nucleophilic attack. Therefore, TsOH was introduced in the reaction system to enhance the formation of enol pyruvate acid. However, only a small peak corresponding to carboxylic acid carbonyl emerged, indicating that a limited number of imine bonds underwent cyclization with PA and subsequent transformation from the enol to the keto tautomer. Nevertheless, the majority of imine bonds within the framework experienced enol to keto tautomerism without undergoing cyclization with PA, as illustrated in (Fig. S2). That was probably because of the poor solubility of the reaction mixture or the rate of enol to keto transformation; however, this riddle was addressed by the addition of DMSO, which effectively solubilized the oligomers as well as TsOH and can influence the kinetics of enol to keto transformation by modulating the polarity and thermodynamics of reaction mixture, allowing adequate time for the cyclization of the appropriate number of enol-imine bonds with PA before it underwent to keto-enamine form. As a result, a prominent peak corresponding to the carboxylic acid carbonyl is observed, demonstrating the successful establishment of sufficient linkage functionality between the framework and PA. Thus, DMSO plays a vital role in the functionalization of COF Tp-Tta-COOH (Fig. S3). However, the DMSO concentration is also crucial for the crystallinity of synthesized COFs. A high concentration of DMSO reduces crystallinity, which might be attributed to the enhanced nucleation rate caused by the high solubility potential of DMSO. After a wide screening of reaction conditions, 1 mL (Dioxane: DMSO) solvent mixture and a catalytic amount of TsOH and glacial acetic acid are set as the optimized reaction parameters for the formation of robust, functionalized, and highly crystalline Tp-Tta-COOH (Figs. S4, 5). This OP three-component strategy was further expanded, and Tp-Tabb-COOH COF was successfully synthesized by the condensation of Tp, Tapb, and PA.

3.1. Characterization

The infrared absorption spectra of Tp-Tta, Tp-Tta-COOH, Tp-Tabb, and Tp-Tabb-COOH was obtained using FT-IR spectroscopy (Fig. 1[B, C]) (Fig. S6). The Tp aldehyde C=O peak at approximately 1636 cm^{-1} , the PA C=O peak at around 1725 cm^{-1} , and the N-H peaks in the range of 3200–3500 cm^{-1} for both Tta and Tapb disappeared after polymerization [12,22]. In contrast, a new carboxylic acid C=O peak emerged at approximately 1713 cm^{-1} in the spectra of Tp-Tta-COOH and Tp-Tabb-COOH, indicating the successful incorporation of the carboxylic acid functional group into the framework via the OP three-component Doebner reaction [30]. Additionally, peaks observed

at approximately 1623 and 1616 cm^{-1} , 1576 and 1572 cm^{-1} , and 1234 and 1256 cm^{-1} can be attributed to the keto $\text{C}=\text{O}$, $\text{C}=\text{C}$, and $\text{C}-\text{N}$ functional groups of Tp-Tta-COOH and Tp-Tapb-COOH, respectively. The presence of enamine ($\text{C}=\text{C}$, $\text{C}-\text{N}$), keto ($\text{C}=\text{O}$), and carboxylic acid carbonyl groups in the FTIR spectrum of Tp-Tta-COOH and Tp-Tapb-COOH provides validation for the proposed reaction mechanism (Fig. S2). Furthermore, the $\text{C}=\text{O}$, $\text{C}=\text{C}$, and $\text{C}-\text{N}$ peaks of Tp-Tta-COOH and Tp-Tapb-COOH closely match with the corresponding peaks of Tp-Tta and Tp-Tapb, confirming the successful formation of β -ketoenamine linkages in Tp-Tta and Tp-Tapb COFs [33–35].

The solid-state ^{13}C NMR spectrum further corroborated the FT-IR results (Fig. S7). The peaks at ~ 183.20 , 183.77, 184.35, and 183.98 ppm were attributed to the keto carbonyl carbons of Tp-Tta, Tp-Tta-COOH, Tp-Tapb, and Tp-Tapb-COOH, respectively. In addition, the peaks at ~ 106.81 , 141.37 ppm; 107.29, 141.48 ppm; 106.93, 146.81 ppm; and 106.65, 146.85 ppm were attributed to the enamine carbons ($\text{C}=\text{C}$, $\text{C}-\text{N}$) of Tp-Tta, Tp-Tta-COOH, Tp-Tapb, and Tp-Tapb-COOH, respectively [34–38]. The resonance signal of carboxylic acid carbonyl carbons were observed at approximately 176.59 and 175.47 ppm in the NMR spectrum of Tp-Tta-COOH and Tp-Tapb-COOH, respectively. In addition, X-ray photoelectron spectroscopy (XPS) was employed to analyze and verify the successful implementation of linkage functionalization via the Doebner reaction (Fig. S8). The peak at a binding energy of 291.2 eV in the high-resolution C 1 s XPS deconvoluted spectra of Tp-Tta-COOH and Tp-Tapb-COOH can be attributed to

the carboxylic acid (COOH) functional group [31,39–41].

The morphology of the prepared COFs was examined by using scanning electron microscopy (SEM). Agglomerated small crystalline particles were observed by SEM [34] (Fig. S9[A–D]). Furthermore, the uniform distribution of C, N, and O in the synthesized COFs was revealed by energy-dispersive spectroscopy mapping (Fig. S9[E–H]). Given the addition of a COOH functional group, the atomic percentage of oxygen in Tp-Tta-COOH and Tp-Tapb-COOH frameworks increased compared with Tp-Tta and Tp-Tapb.

PXRD was utilized in order to evaluate the crystallinity of the synthesized COFs (Fig. 2[A–D]). Three distinct peaks were observed in the PXRD profile of Tp-Tta (at 2θ value of 5.63° , 9.65° , and 26.55°), Tp-Tta-COOH (5.33° , 9.69° , and 25.95°), Tp-Tapb (5.62° , 10.17° , and 25.66°), and Tp-Tapb-COOH (5.66° , 10.16° , and 25.46°) corresponding to the (100), (110), and (001) planes, respectively. The broad peak around 26° might be associated with π - π stacking. The profile differences and low residual values ($R_{\text{wp}} \leq 5.05\%$ and $R_p \leq 3.88\%$) indicated that the simulated PXRD patterns of eclipsed (AA) stacking structures correlate well with the experimental data (Tables S1–4) [42].

The surface area and porosity of the constructed COFs were assessed using N_2 sorption isotherms at a temperature of 77 K. Tp-Tta, Tp-Tapb, Tp-Tta-COOH, and Tp-Tapb-COOH were each determined to have BET surface areas of 1012, 686.47, 446.65, and $61.80 \text{ m}^2/\text{g}$, respectively (Fig. S10[A–D]). The reduction in surface area of modified COF materials can be attributed to several factors, including irreversible PA-

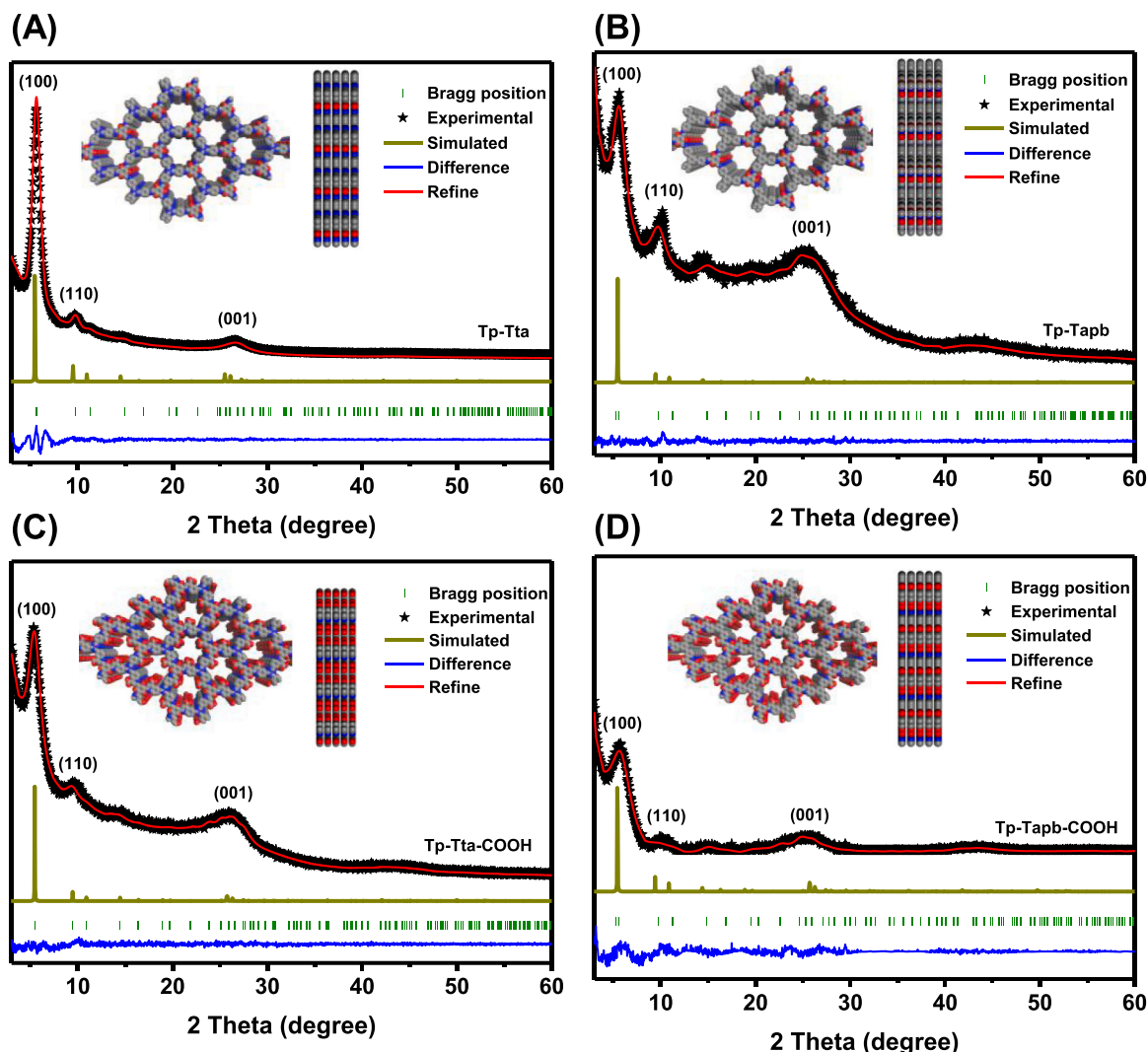


Fig. 2. PXRD patterns of COFs (A–D) (inset: top and side view).

induced cyclization of the imine bond, a higher mass per repeating unit, reduced pore size, and lower crystallinity, particularly pronounced in the case of Tp-Tapb-COOH [12,31,43]. The assessment of pore-size distribution was conducted through the application of nonlocal density functional theory, revealing a narrow distribution across all COFs. The primary pore sizes of Tp-Tta, Tp-Tapb, Tp-Tta-COOH, and Tp-Tapb-COOH were measured to be approximately 1.5 nm, 1.3 nm, 1.07 nm, and 1.07 nm, respectively. These measurements closely align with values calculated from simulated structures (Fig. S11[A–D]) [34, 44]. Notably, Tp-Tapb exhibits a slightly smaller experimental pore size compared to the theoretically calculated one, which could be attributed to the intergrowth of COF particles within the pores leading to a reduction in the experimental pore size [45]. Furthermore, the reduction in pore size was observed following the linkage modification, as it becomes integrated into the pore space [13,31]. A thermogravimetric study showed that all of the synthesized COFs had excellent thermal stability (Fig. S12[A–D]).

COF Tp-Tta and its functionalized analog Tp-Tta-COOH were selected as the model materials to determine the effect of linkage functionalization on chemical stability in acid and base solutions. Although β -ketoenamine linkages have reasonable stability in acid and base solutions, cyclization further enhanced the chemical stability particularly toward acids (e.g., concentrated H_2SO_4). The FT-IR and PXRD spectra of Tp-Tta-COOH after acid/base treatment demonstrated functional group durability and adequate crystallinity, but the FT-IR spectra of Tp-Tta after treatment with H_2SO_4 exhibited N-H and C-H peaks resulting from the acid hydrolysis of the enamine linkage (Fig. 3 [A–D]) (Fig. S13). Thus, Tp-Tta-COOH showed superior chemical

stability because of linkage functionalization than Tp-Tta under severe conditions, which promotes the efficacy of materials in real-world applications.

The optical properties of synthesized materials were also analyzed. Tp-Tta, Tp-Tapb, Tp-Tta-COOH, and Tp-Tapb-COOH exhibited an absorption edge of ~ 542 , 556, 597, and 635 nm, respectively, in the ultraviolet (UV)–visible (VIS) DRS optical absorption spectra (Fig. 4[A]) [46].

The band gap (E_g) energy of the given sample was determined using the Kubelka-Munk method (Eq. 1), and the optical band gaps for Tp-Tta, Tp-Tapb, Tp-Tta-COOH, and Tp-Tapb-COOH were determined to be 2.4, 2.41, 2.32, and 2.31 eV, respectively (Fig. 4[B]).

$$\alpha(h\nu) = A(h\nu - E_g)^{1/2} \quad (1)$$

Thus, Tp-Tta-COOH and Tp-Tapb-COOH exhibited enhanced VIS light absorption and decreased band gap caused by linkage functionalization that extended π conjugation in the framework. The synthesized COFs were n-type semiconductors as evidenced by the positive slope of Mott-Schottky (M-S) graphs measured at 464, 1000, and 1468 Hz. Extrapolating the M-S plots, approximately -0.63 , -0.66 , -0.72 , and -0.68 eV vs. Ag/AgCl were obtained for the flat band (FB) potential of Tp-Tta, Tp-Tapb, Tp-Tta-COOH, and Tp-Tapb-COOH, respectively (Fig. S14[A–D]) [46,47]. The conduction band (CB) position of an n-type semiconductor is 0.2 more negative than the FB position. Thus, the CB was calculated as -0.63 , -0.66 , -0.72 , and -0.68 eV vs. NHE in accordance with Eq. 2 [37]. Afterward, the valence band (VB) potential was calculated as 1.77, 1.75, 1.60, and 1.63 eV for Tp-Tta,

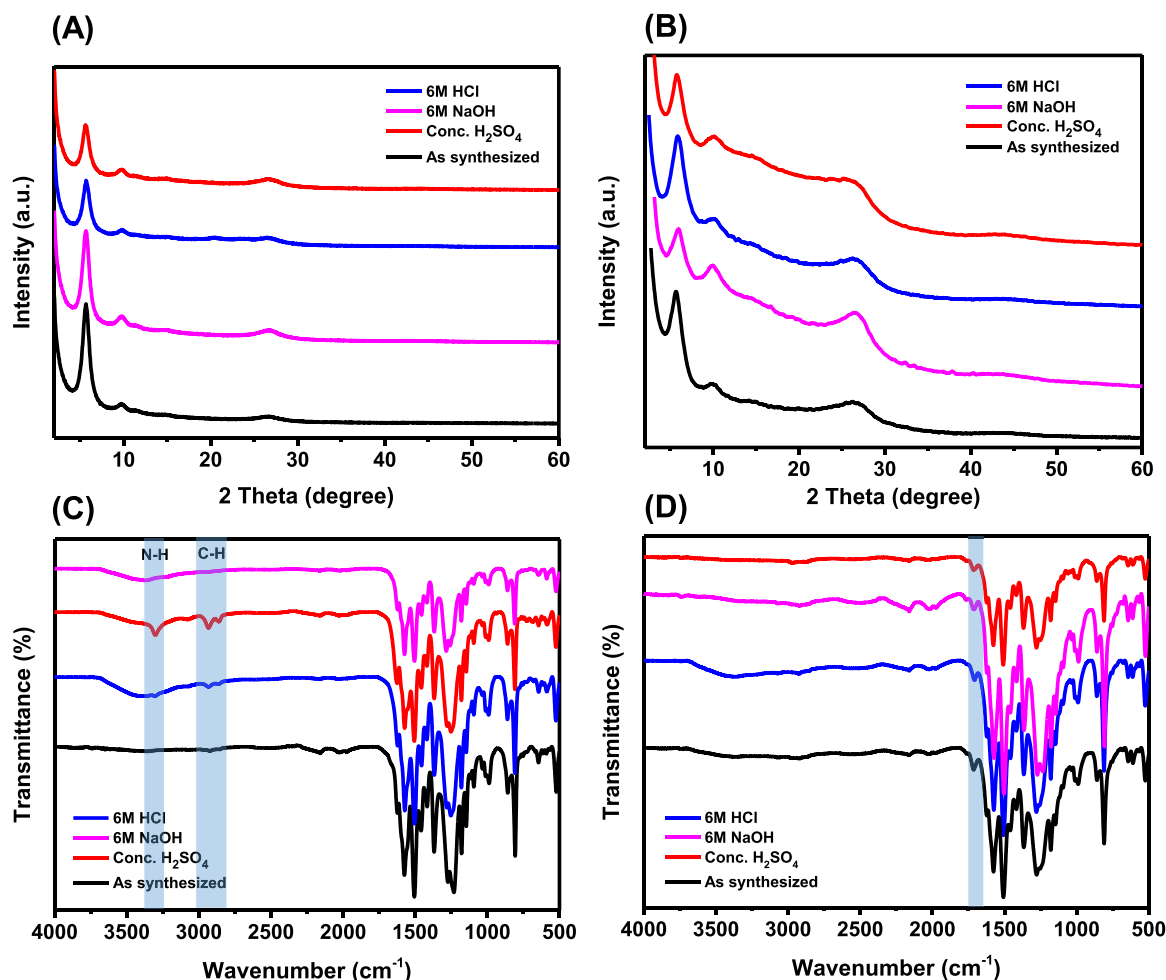


Fig. 3. PXRD patterns and FT-IR spectra of (A, C) Tp-Tta and (B, D) Tp-Tta-COOH after soaking in different solutions.

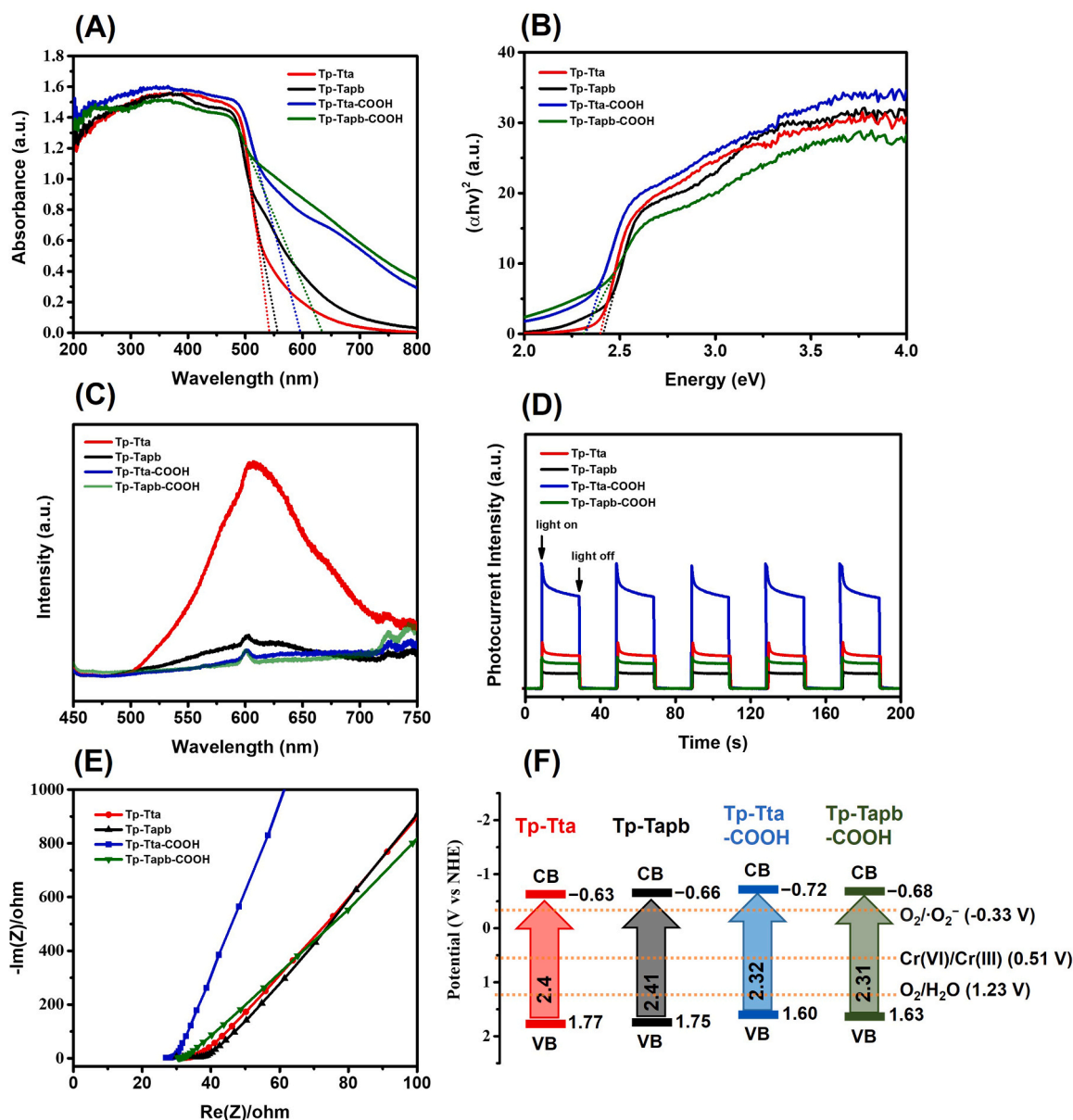


Fig. 4. (A) UV-vis DRS spectra, (B) Tauc plots, (C) Photoluminescence spectra (excitation wavelength = 400 nm), (D) Transient photocurrent response spectra, (E) Nyquist plots from electrochemical impedance spectra, and (F) Band structure diagrams of all COFs (dashed lines shows the potential of $\text{O}_2/\bullet\text{O}_2^-$, Cr(VI)/Cr(III) , and $\text{O}_2/\text{H}_2\text{O}$).

Tp-Tapb, Tp-Tta-COOH, and Tp-Tapb-COOH, respectively, in accordance with Eq. 3.

$$E_{\text{NHE}} = E_{\text{Ag/AgCl}} + E_{\text{Ag/AgCl}}^0 \quad (E_{\text{Ag/AgCl}}^0 = 0.1976 \text{ eV}) \quad (2)$$

$$E_g = E_{\text{VB}} - E_{\text{CB}} \quad (3)$$

The VB XPS approach was used to obtain considerable evidence for the relative VB position of Tp-Tta, Tp-Tapb, Tp-Tta-COOH, and Tp-Tapb-COOH (Fig. S15) [48]. The CB potential of synthesized COFs is more negative than the Cr(VI)/Cr(III) reduction potential (0.51 V), indicating their capability to reduce Cr(VI) to Cr(III) [49].

The electron-hole pair separation and recombination efficiency of synthesized COFs was evaluated on the basis of the photoluminescence (PL) emission spectra. The PL intensity of Tp-Tta-COOH and Tp-Tapb-COOH was depressed compared with Tp-Tta and Tp-Tapb (Fig. 4[C]). Therefore, the incorporation of an electron-withdrawing carboxylic acid functional group via cyclization of an imine bond with PA could promote charge transfer and suppress the recombination of photoinduced

electron-hole pairs. Furthermore, transient photocurrent responses and electrochemical impedance spectroscopy were used to examine the effect of the material structure on charge mobility. As shown in Fig. 4[D], Tp-Tta-COOH and Tp-Tapb-COOH displayed significantly bigger photocurrents than Tp-Tta and Tp-Tapb, indicating that they were more effective at generating, splitting, and transferring charge carriers. Moreover, Tp-Tta-COOH exhibited the lowest charge transfer resistance among the synthesized COFs (Fig. 4[E]).

Density functional theory using the B3LYP/3-21 G approach was used to compute the frontier molecular orbital of COFs (Fig. S16[A-D]). LUMO of synthesized COFs were primarily located at the electron-withdrawing ketoenamine units, while their HOMO were mainly located at the electron rich benzene rings. Tp-Tta, Tp-Tta-COOH, Tp-Tapb, and Tp-Tapb-COOH have theoretical HOMO/LUMO energy levels of $-6.791/-1.532$, $-6.935/-1.883$, $-6.637/-1.462$, and $-6.775/-1.849$, respectively. Therefore, the electrochemical band gaps were calculated to be 5.25, 5.05, 5.17, and 4.93 eV, respectively,

which were relative to the optical band gaps. However, estimated energy gaps were greater than experimental ones, possibly because the chosen model was the single repeating unit without taking into account the layer stacking and extension of COF materials [50]. These theoretical studies demonstrate the impact of linkage functionalization, and a lowered electrochemical band gap was observed for functionalized COFs compared with their unfunctionalized analogs. The linkage functionalization in Tp-Tta-COOH and Tp-Tapb-COOH resulted in enhanced VIS light absorption, decreased band gap, lowered charge transfer resistance, and improved electron-hole pair production, separation, and transmission efficiency. These findings indicate that the synthesized COFs could be used as photocatalysts for the elimination of Cr(VI) pollution.

3.2. Adsorption-photocatalysis synergy for Cr(VI) removal

After elucidating all the structural, optical, electrochemical, and photoelectrochemical properties using high-end characterization techniques, the adsorption-photocatalytic reduction activity of synthesized adsorbent materials was studied by measuring the Cr(VI) removal rates in the presence/absence of light. We set out to create a hybrid strategy that relied on adsorption and photocatalysis techniques for efficient Cr(VI) removal from water. Tp-Tta, Tp-Tapb, Tp-Tta-COOH, and Tp-Tapb-COOH were compared with regard to their ability to remove Cr(VI) from the solution (Fig. 5[A]). During the dark phase, Tp-Tta, Tp-Tapb, Tp-Tta-COOH, and Tp-Tapb-COOH eliminated Cr(VI) from the solution by

adsorption. The adsorption equilibrium was almost attained in 60 min, and the adsorption percentages at 60 min were 21%, 37%, 39%, and 42% (Fig. S17). Tta monomer has a planar structure compared with Tapb. Thus, Tapb monomer-based COFs, such as Tp-Tapb and Tp-Tapb-COOH, have higher interlayer spacing than Tp-Tta and Tp-Tapb [51,52]. Given their high interlayer spacing, more binding sites have been exposed, which leads to higher Cr(VI) adsorption for Tp-Tapb and Tp-Tapb-COOH as compared with Tp-Tta and Tp-Tta-COOH, respectively. Moreover, Cr(VI) removal via adsorption increased with the insertion of the carboxylic acid functional groups in the framework, which can actively coordinate with Cr(VI) [53]. Upon light irradiation, Tp-Tta, Tp-Tapb, Tp-Tta-COOH, and Tp-Tapb-COOH catalyzed the photoreduction of Cr(VI) to Cr(III), resulting in a decrease in the concentration of Cr(VI). After 120 min, the Cr(VI) removal percentage of Tp-Tta, Tp-Tapb, Tp-Tta-COOH, and Tp-Tapb-COOH was 64%, 59%, 99.8%, and 82%, respectively. Under light, Tp-Tta-COOH and Tp-Tapb-COOH were able to remove Cr(VI) more effectively than their unfunctionalized counterparts Tp-Tta and Tp-Tapb because of their ability to efficiently harvest photons, narrower band gap, and higher charge mobility. Tp-Tta and Tp-Tta-COOH exhibited better photoreduction than Tp-Tapb and Tp-Tapb-COOH, respectively, because of the inclusion of an electron-deficient triazine ring that facilitates the electron-hole pair separation [36]. Therefore, Tp-Tta-COOH is a remarkable metal-free photocatalyst that can quickly and effectively remove > 99% Cr(VI) without using a scavenger (Fig. 5[B]).

Based on prior experimental results, Tp-Tta-COOH was selected for

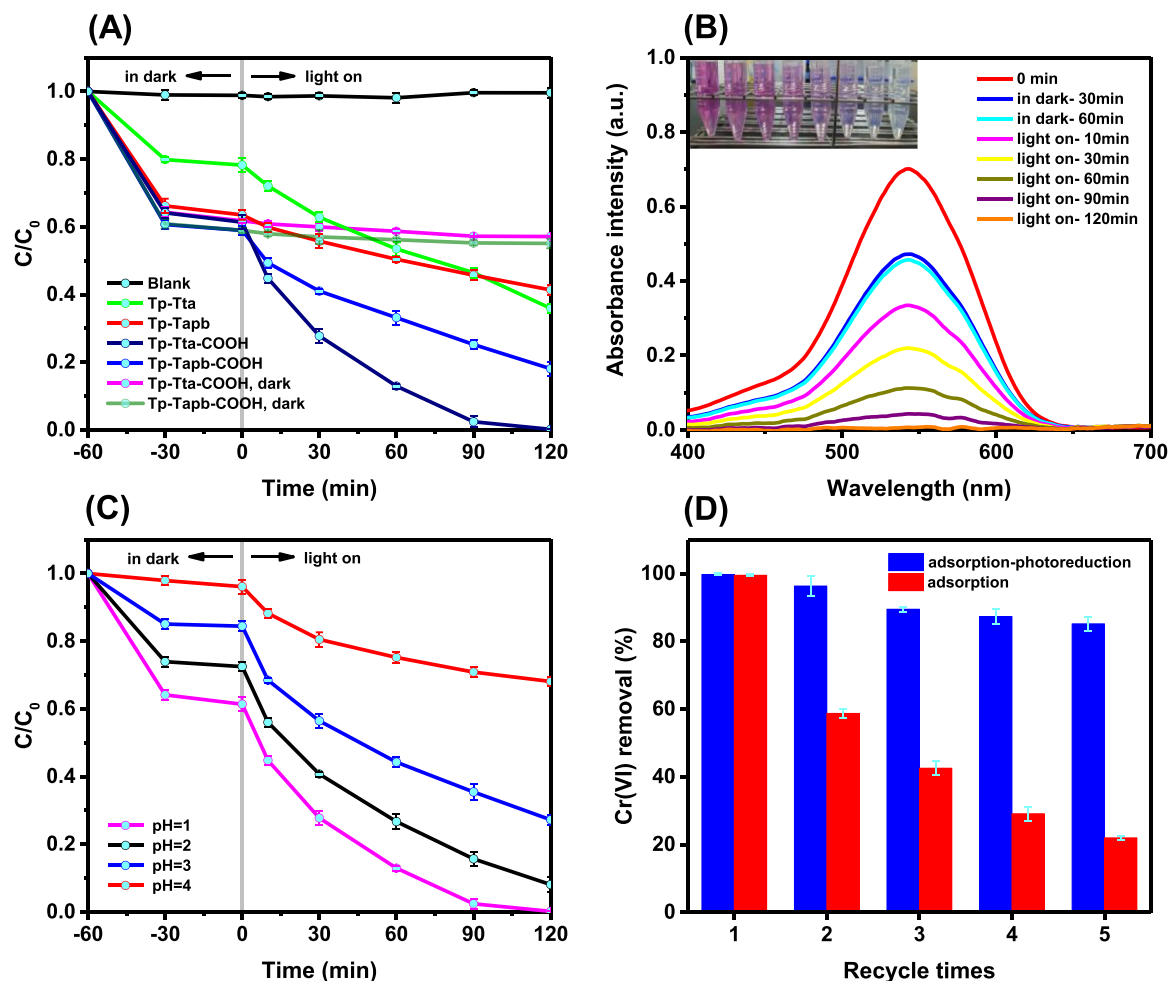
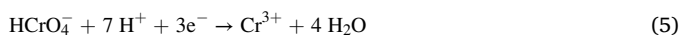
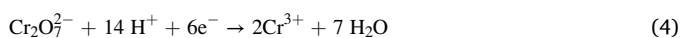


Fig. 5. (A) Comparison of COFs for Cr(VI) removal via adsorption-photocatalytic reduction, (B) UV-Vis spectroscopy of Cr(VI) solutions at different time points in the presence of Tp-Tta-COOH, (C) Cr(VI) removal performance of Tp-Tta-COOH at different pH, and (D) Recycling runs of Tp-Tta-COOH in removing Cr(VI) without desorption.

further investigation because of its superior performance in the removal of Cr(VI) via the synergy of the adsorption–photoreduction approach. The distribution of chromium species in the solution as well as the surface charge and degree of protonation of the adsorbent were all affected by the solution pH, making the adsorption and photoreduction of Cr(VI) by Tp-Tta-COOH extremely pH-dependent processes (Fig. 5 [C]). The adsorption and photoreduction effectiveness of Cr(VI) removal decreased with the increase of the initial pH of solutions. At solution pH of 1, adsorption removed 39% and photoreduction removed 60.8%, resulting in more than 99% Cr(VI) removed from the solution via adsorption–photoreduction synergy. At pH of 4, Cr(VI) removal by adsorption and photoreduction accounted for only 4% and 31.8%, respectively. Therefore, Cr(VI) removal by Tp-Tta-COOH is most effective at pH 1. A high concentration of H^+ in solution (1) protonates the heteroatoms (N, O) of Tp-Tta-COOH, resulting in an electrostatic interaction between Tp-Tta-COOH cationic species and Cr(VI) anionic species ($Cr_2O_7^{2-}$ and $HCrO_4^-$ at pH = 1) and (2) potentially improves Cr(VI) reduction performance by accelerating the conversion from Cr(VI) to Cr(III) that can be elucidated by the Eqs. 4 and 5 [14,19,54,55].



The remarkable Cr(VI) removal capacity of Tp-Tta-COOH at a low dosage stands out compared with other reported materials (Table S5). Moreover, Tp-Tta-COOH was examined for its ability to remove Cr(VI) from H_2SO_4 solutions (Fig. S18). In the case of a 1 M H_2SO_4 chromium solution, 39.6% of Cr(VI) was removed through an adsorption–chemical reduction process in the dark. However, when exposed to light, Tp-Tta-COOH catalyzed the photoreduction of Cr(VI) to Cr(III), achieving over 99% Cr(VI) removal within 120 min. As the concentration of H_2SO_4 increased, the conversion of Cr(VI) to Cr(III) via chemical reduction also increased (Eqs. 4, 5) [56,57]. Notably, over 99% of Cr(VI) was removed within 30 min via chemical reduction from the highly acidic 9 M H_2SO_4 chromium solution. To the best of our knowledge, Tp-Tta-COOH is the

first material reported to successfully remove Cr(VI) under such severe acidic conditions (9 M H_2SO_4). Furthermore, UV and VIS light were tested for their ability to facilitate Cr(VI) removal by Tp-Tta-COOH and were shown to be equally efficient (Fig. S19).

The ability to recycle is crucial for the viable utilization of photocatalysis. Tp-Tta-COOH recycling runs for removing Cr(VI) were assessed (Fig. 5[D]). Without any elution or desorption, subsequent cycle runs occur after each cycle run. Two processes, adsorption and adsorption–photoreduction, were carried out. Only around 22% of the Cr(VI) removal capacity was left after adsorption for 5 cycles, indicating that Cr(VI) had already occupied the adsorption sites and could not be moved any further. Although the removal ability of Cr(VI) decreased to a certain extent after each cycle run in the adsorption–photoreduction process because of the deposition of Cr species on the Tp-Tta-COOH surface, > 85% of the removal capacity was maintained after five cycle runs. Thus, adsorbed Cr(VI) was further reduced to Cr(III) through photocatalysis by Tp-Tta-COOH and then returned to solution due to the electrostatic repulsion between cationic Cr(III) and positive surface charge of Tp-Tta-COOH, ensuring the availability of catalyst's active sites for the subsequent cycle run (Fig. S20). The synergy of adsorption and photoreduction remarkably enhanced the reusability of Tp-Tta-COOH. Furthermore, after undergoing five cycles of adsorption and photoreduction, Tp-Tta-COOH maintained its structural integrity, as evidenced by FT-IR and XRD spectra (Fig. S21[A, B]) [26].

3.3. Cr(VI) removal mechanism

The XPS spectra of Tp-Tta-COOH were measured before and after adsorption and photoreduction to obtain insight into the removal mechanism, and the existence of Cr 2p peaks in the survey spectra indicated that Cr species had been successfully adsorbed (Fig. 6[B]). After adsorption and photoreduction, Cr 2p spectra of Tp-Tta-COOH could be split into two components, ascribing to Cr(VI) and Cr(III) ions [58]. After adsorption, Cr(VI) (577.9 and 587.2 eV) and Cr(III) (576.7 and 586.3 eV) accounted for the majority and minority of the

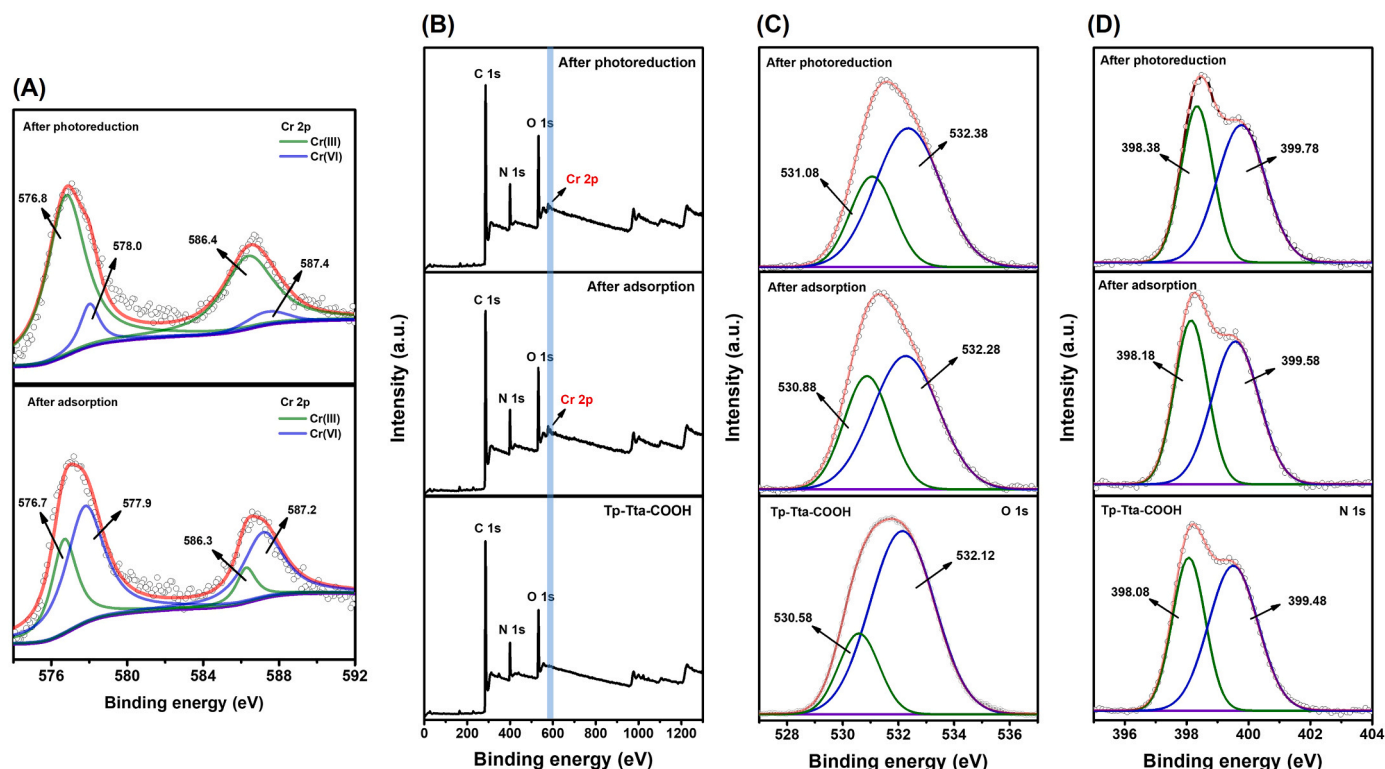


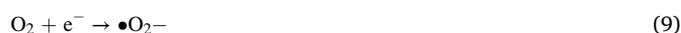
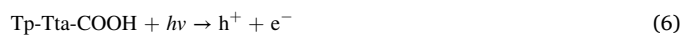
Fig. 6. (A) XPS component peak-fitting spectra of Cr 2p; (B) wide scan XPS spectrum; (C, D) XPS component peak-fitting spectra of N 1s and O 1s.

deconvoluted spectra of Cr 2p, respectively (Fig. 6[A]). The presence of Cr(III) showed that the framework could partially reduce Cr(VI) to Cr(III) through chemical reduction (Fig. S22) [14]. Nevertheless, following photoreduction, the deconvoluted XPS spectrum in the Cr 2p region exhibited notable peaks at 576.8 and 586.4 eV, which were attributed to Cr(III). In addition, broad low peaks at 578.0 and 587.4 eV were observed, likely indicative of the presence of a small amount of Cr(VI) (Fig. 6[A]). The presence of unconverted residual Cr(VI) on COF surface or reoxidation of some of the created Cr(III) by photogenerated h^+ or 1O_2 may account for the appearance of low Cr(VI) peaks in the deconvoluted XPS spectrum [36]. The O 1s XPS spectra exhibit typical peaks at 530.78 and 532.48 eV, which correspond to C=O and C-OH moieties, respectively (Fig. 6[C]). After adsorption and photoreduction, a significant binding energy change was detected, which was attributed to the interaction of carbonyl and carboxylic acid O atoms with the Cr species. Similarly, the N 1s spectra show a shift in the location of the C-N/N-H (399.48 eV) and C-C=N (398.08 eV) peaks toward a higher binding energy, indicating that the N atoms of enamine and triazine moieties interacted with Cr species during adsorption and photoreduction (Fig. 6[D]) [36,42,59,60].

Through capture experiments and Electron Spin Resonance (ESR), we investigated the components involved in the photoreduction of Cr(VI) and the potential photocatalytic pathway of Tp-Tta-COOH (Figs. S23 and S24). As part of our investigations, we employed potassium persulfate ($K_2S_2O_8$) and silver nitrate ($AgNO_3$) as scavengers for electrons (e^-), while p-benzoquinone (PBQ) and isopropyl alcohol (IPA) were utilized as scavengers for superoxide radicals ($\bullet O_2^-$) and hydroxyl radicals ($\bullet OH$), respectively [15,61–65]. For scavenging holes (h^+), we employed methanol and benzyl alcohol (BA) [54,55]. When $K_2S_2O_8$ and $AgNO_3$ were introduced, the efficiency of Cr(VI) photoreduction on Tp-Tta-COOH notably decreased, suggesting that electrons (e^-) were the primary active species. Additionally, a slight reduction in the efficiency of Cr(VI) photoreduction was observed upon the addition of PBQ, indicating the influence of superoxide radicals ($\bullet O_2^-$) on the reduction process. Furthermore, upon irradiation, signals of DMPO- $\bullet O_2^-$ and TEMPO- h^+ were detected in the ESR spectrum (Fig. S25[A,B]). This implies that in the presence of Cr(VI), the majority of electrons underwent a direct and predominant reduction of Cr(VI) to Cr(III), while a smaller fraction of electrons engaged in a reaction with O_2 , resulting in the formation of $\bullet O_2^-$, which also contributed in the reduction of Cr(VI) to Cr(III) [61,66]. The $O_2/\bullet O_2^-$ has a potential of -0.33 V, and the CB of Tp-Tta-COOH is positioned at an adequate negative value to facilitate the generation of $\bullet O_2^-$ – [67,68]. However, the efficiency of Cr(VI) photocatalytic reduction was found to increase upon the removal of O_2 from the system. This leads us to the notion that a significant amount of O_2 present in the solution might result from the oxidation of water molecules by photogenerated holes. The potential of the O_2/H_2O is measured to be 1.23 V and Tp-Tta-COOH has a sufficiently positive valence band (VB) to facilitate the oxidation of water via Eq. 8 [67,69]. So, O_2 exclusion urges the water oxidation process that assists the dissociation of electron-hole pairs, thus leading to an enhancement in the Cr(VI) photocatalytic reduction [67]. Moreover, the addition of methanol and BA increased the Cr(VI) reduction rate because the scavengers effectively consume the photoinduced holes and suppress the electron-hole pairs recombination that resulted in the improved availability of e^- for the Cr(VI) photocatalytic reduction [54,55]. While the presence of IPA did not affect the Cr(VI) reduction efficiency showing that $\bullet OH$ is not the active specie in this system. Moreover, the DMPO- $\bullet OH$ signal was not observed in the ESR spectrum after irradiation (Fig. S25[C]). Further evidence that $\bullet OH$ is not being generated in the photocatalytic process was provided by the absence of fluorescence emission of 2-hydroxy-terephthalic acid (TAOH) at 426 nm after the addition of terephthalic acid (TA) to the Tp-Tta-COOH system as TAOH is formed by the reaction of $\bullet OH$ with TA (Fig. S26) [21,25,70]. The potential of the $\bullet OH/H_2O$ is 2.73 V, indicating the VB potentials of Tp-Tta-COOH were unfavorable for the production of $\bullet OH$ [71,72].

Based on the ESR and radical trapping test data, it can be deduced that the Cr(VI) was reduced by the photogenerated electrons e^- and $\bullet O_2^-$ radicals.

The above discussion and analysis suggest that the photocatalytic mechanism behind this study's findings can be described by the equations (Eq. 6) through (Eq. 10).



The mechanism of Cr(VI) removal on Tp-Tta-COOH is illustrated in Fig. 7, which can be summarized into the following points based on the preceding experimental data; (1) The adsorption of anionic Cr(VI) species ($Cr_2O_7^{2-}$ & $HCrO_4^-$) onto the Tp-Tta-COOH surface occurred through electrostatic interaction between the protonated functional groups of Tp-Tta-COOH and Cr(VI) [73]. (2) The electron-rich groups of Tp-Tta-COOH facilitated the conversion of Cr(VI) to Cr(III) via chemical reduction. (3) Under light exposure, electron-hole pairs were generated; most electrons (e^-) directly participated in the reduction of Cr(VI) to Cr(III), while some were consumed by O_2 , producing superoxide radicals ($\bullet O_2^-$), which also contributed to Cr(VI) reduction to some extent. Simultaneously, the holes might took part in water oxidation [67,69,74]. (4) Due to electrostatic repulsion between the newly formed cationic Cr(III) and the positive surface charge of Tp-Tta-COOH at low pH, a significant portion of the reduced Cr(III) returned to the solution [14,70].

4. Conclusion

The three-component Doebner reaction was used to develop novel porous, crystalline, carboxylic acid-functionalized Tp-Tta-COOH and Tp-Tapb-COOH COFs. Tp-Tta and Tp-Tapb, as well as their unfunctionalized counterparts, were also synthesized to evaluate and compare the effect of linkage functionalization on structural characteristics and Cr(VI) removal. The inclusion of COOH-chelating groups, tremendous chemical stability, permanent porosity, recycling ability, enhanced absorption of VIS light, reduced band gap, lowered charge transfer resistance, and improved efficiency in producing, separating, and transmitting electron-hole pairs endowed by linkage functionalization, Tp-Tta-COOH exhibited tremendous Cr(VI) removal performance via adsorption-photoreduction synergy. Therefore, this manner of functionalization in β -ketoenamine-linked COFs with diverse assembly has significant potential in various applications such as Cr(VI) removal.

CRedit authorship contribution statement

Lee Dae Sung: Conceptualization, Project administration, Resources, Software, Supervision, Validation, Visualization, Writing – review & editing. **Cheong In Woo:** Supervision, Validation. **Kim Bolam:** Conceptualization, Data curation, Formal analysis, Investigation, Methodology, Validation. **Devarayapalli Kamakshiah:** Conceptualization, Data curation, Formal analysis, Investigation, Methodology, Validation. **Saddique Anam:** Data curation, Formal analysis, Methodology. **Hussain Muzammil:** Conceptualization, Data curation, Formal analysis, Investigation, Methodology, Writing – original draft.

Declaration of Competing Interest

The authors declare that they have no known competing financial interests or personal relationships that could have appeared to influence the work reported in this paper.

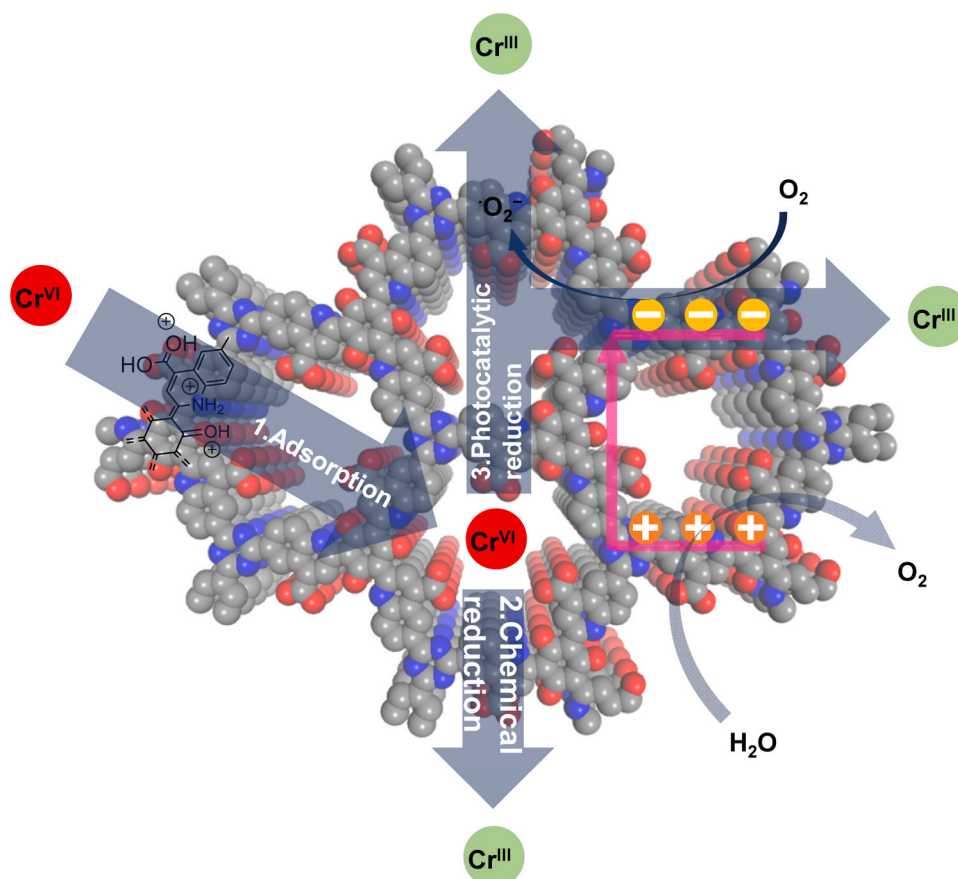


Fig. 7. The proposed mechanism of Cr(VI) removal on Tp-Tta-COOH.

Data availability

Data will be made available on request.

Acknowledgements

This research was supported by the Basic Science Research Program through the National Research Foundation of Korea (NRF), funded by the Ministry of Education (NRF-2018R1A6A1A03024962) and the Ministry of Science and ICT (NRF-2020R1A2C2100746).

Appendix A. Supporting information

Supplementary data associated with this article can be found in the online version at [doi:10.1016/j.apcatb.2023.123672](https://doi.org/10.1016/j.apcatb.2023.123672).

References

- [1] K. Geng, T. He, R. Liu, S. Dalapati, K.T. Tan, Z. Li, S. Tao, Y. Gong, Q. Jiang, D. Jiang, Covalent organic frameworks: design, synthesis, and functions, *Chem. Rev.* 120 (2020) 8814–8933.
- [2] S. Zhuo, X. Wang, L. Li, S. Yang, Y. Ji, Chiral carboxyl-functionalized covalent organic framework for enantioselective adsorption of amino acids, *ACS Appl. Mater. Interfaces* 13 (2021) 31059–31065.
- [3] S. Karak, S. Kumar, P. Pachfule, R. Banerjee, Porosity prediction through hydrogen bonding in covalent organic frameworks, *J. Am. Chem. Soc.* 140 (2018) 5138–5145.
- [4] R. Wang, W. Kong, T. Zhou, C. Wang, J. Guo, Organobase modulated synthesis of high-quality β -ketoenamine-linked covalent organic frameworks, *Chem. Commun.* 57 (2021) 331–334.
- [5] B.P. Biswal, S. Kandambeth, S. Chandra, D.B. Shinde, S. Bera, S. Karak, B. Garai, U. K. Kharul, R. Banerjee, Pore surface engineering in porous, chemically stable covalent organic frameworks for water adsorption, *J. Mater. Chem. A* 3 (2015) 23664–23669.
- [6] Y. Pang, B. Wang, Y. Kang, J. Li, X. Gu, G. Kang, X. Yan, Y. Li, L. Chen, Sulfonated chiral covalent organic frameworks-mediated asymmetric Michael addition of acetone to β -nitroolefins, *Chem. Eng. Sci.* 260 (2022) 117933.
- [7] Y. Peng, G. Xu, Z. Hu, Y. Cheng, C. Chi, D. Yuan, H. Cheng, D. Zhao, Mechanoassisted synthesis of sulfonated covalent organic frameworks with high intrinsic proton conductivity, *ACS Appl. Mater. Interfaces* 8 (2016) 18505–18512.
- [8] S.P.S. Fernandes, A. Mellah, P. Kovár, M.P. Sárria, M. Pšenicka, H. Djamila, L. M. Salonen, B. Espiña, Extraction of ibuprofen from natural waters using a covalent organic framework, *Molecules* 25 (2020) 3132.
- [9] P.L. Wang, S.Y. Ding, Z.C. Zhang, Z.P. Wang, W. Wang, Constructing robust covalent organic frameworks via multicomponent reactions, *J. Am. Chem. Soc.* 141 (2019) 18004–18008.
- [10] K. Wang, Z. Jia, Y. Bai, X.X. Wang, S.E. Hodgkiss, L. Chen, S.Y. Chong, X.X. Wang, H. Yang, Y. Xu, F. Feng, J.W. Ward, A.I. Cooper, Synthesis of stable thiazole-linked covalent organic frameworks via a multicomponent reaction, *J. Am. Chem. Soc.* 142 (2020) 11131–11138.
- [11] P.F. Wei, M.Z. Qi, Z.P. Wang, S.Y. Ding, W. Yu, Q. Liu, L.K. Wang, H.Z. Wang, W. K. An, W. Wang, Benzoxazole-linked ultrastable covalent organic frameworks for photocatalysis, *J. Am. Chem. Soc.* 140 (2018) 4623–4631.
- [12] X.T. Li, J. Zou, Q. Yu, Y. Liu, J.R. Li, M.J. Li, H.C. Ma, G.J. Chen, Y. Bin Dong, Construction of acid–base bifunctional covalent organic frameworks via Doebner reaction for catalysing cascade reaction, *Chem. Commun.* 58 (2022) 2508–2511.
- [13] Y. Yang, L. Yu, T. Chu, H. Niu, J. Wang, Y. Cai, Constructing chemical stable 4-carboxyl-quinoline linked covalent organic frameworks via Doebner reaction for nanofiltration, *Nat. Commun.* 131 (13) (2022) 1–9.
- [14] X. Zhong, Z. Lu, W. Liang, B. Hu, The magnetic covalent organic framework as a platform for high-performance extraction of Cr(VI) and bisphenol A from aqueous solution, *J. Hazard. Mater.* 393 (2020) 122353.
- [15] W.Y. Geng, F.Y. Chen, Y.H. Luo, Z.Y. Liu, S.F. Guo, Y.Y. Zhang, D.E. Zhang, X.Y. Yu, Boosting photocatalytic Cr(VI) reduction activities of layered COF through regulating donor-acceptor units and the orientation of imine bonds, *Microporous Mesoporous Mater.* 351 (2023) 112479.
- [16] C.M. Stern, T.O. Jegede, V.A. Hulse, N. Elgrishi, Electrochemical reduction of Cr(VI) in water: lessons learned from fundamental studies and applications, *Chem. Soc. Rev.* 50 (2021) 1642–1667.
- [17] G. Zolfaghari, M. Kargar, Nanofiltration and microfiltration for the removal of chromium, total dissolved solids, and sulfate from water, *Methods X* 6 (2019) 549–557.
- [18] G. Almaguer-Busso, G. Velasco-Martínez, G. Carreño-Aguilera, S. Gutiérrez-Granados, E. Torres-Reyes, A. Alatorre-Ordaz, A comparative study of global

- hexavalent chromium removal by chemical and electrochemical processes, *Electrochem. Commun.* 11 (2009) 1097–1100.
- [19] D. Zhu, S. Zhou, Z. Zhou, R. Li, J. Ye, X. Ziyu, S. Lan, Y. Zhang, S. Miao, W. Wang, Highly efficient and selective removal of Cr(VI) by covalent organic frameworks: structure, performance and mechanism, *Colloids Surf. A Physicochem. Eng. Asp.* 600 (2020) 124910.
- [20] Y. Xing, X. Chen, D. Wang, Electrically regenerated ion exchange for removal and recovery of Cr(VI) from wastewater, *Environ. Sci. Technol.* 41 (2007) 1439–1443.
- [21] J.Y. Yue, Y.T. Wang, X.L. Ding, Y.F. Fan, L.P. Song, P. Yang, Y. Ma, B. Tang, Single-atom substitution in donor-acceptor covalent organic frameworks for tunable visible light photocatalytic Cr(VI) reduction, *Mater. Chem. Front.* 6 (2022) 3748–3754.
- [22] M. Hussain, N. Maile, K. Tahir, A.A. Ghani, B. Kim, J. Jang, D.S. Lee, Flexible thiourea-based covalent organic frameworks for ultrahigh mercury removal from aqueous solutions, *Chem. Eng. J.* 446 (2022) 137410.
- [23] Z. Xia, Y. Zhao, S.B. Darling, Z. Xia, S.B. Darling, Y. Zhao, Covalent organic frameworks for water treatment, *Adv. Mater. Interfaces* 8 (2021) 2001507.
- [24] V.D. da Silva, K. Zalewska, Z. Petrovski, C.D. Buarque, L.C. Branco, P.M. Esteves, Covalent organic frameworks as promising materials for the removal of metal and organic pollutants from water, *Mater. Today Sustain.* 21 (2023) 100279.
- [25] F. Liu, Z. Ma, Y. Deng, M. Wang, P. Zhou, W. Liu, S. Guo, M. Tong, D. Ma, Tunable covalent organic frameworks with different heterocyclic nitrogen locations for efficient Cr(VI) reduction, *escherichia coli* disinfection, and paracetamol degradation under visible-light irradiation, *Environ. Sci. Technol.* 55 (2021) 5371–5381.
- [26] W. Chen, Z. Yang, Z. Xie, Y. Li, X. Yu, F. Lu, L. Chen, Benzothiadiazole functionalized D-A type covalent organic frameworks for effective photocatalytic reduction of aqueous chromium(VI), *J. Mater. Chem. A* 7 (2019) 998–1004.
- [27] S. Jansone-Popova, A. Moine, J.A. Schott, S.M. Mahurin, I. Popovs, G.M. Veith, B. A. Moyer, Guanidinium-based ionic covalent organic framework for rapid and selective removal of toxic Cr(VI) oxoanions from water, *Environ. Sci. Technol.* 53 (2019) 883.
- [28] M. Nawaz, A. Shahzad, K. Tahir, J. Kim, M. Moztahida, J. Jang, M.B. Alam, S. H. Lee, H.Y. Jung, D.S. Lee, Photo-Fenton reaction for the degradation of sulfamethoxazole using a multi-walled carbon nanotube-NiFe₂O₄ composite, *Chem. Eng. J.* 382 (2020) 123053.
- [29] M. Moztahida, D.S. Lee, Photocatalytic degradation of methylene blue with P25/graphene/polyacrylamide hydrogels: optimization using response surface methodology, *J. Hazard. Mater.* 400 (2020) 123314.
- [30] L.-G.G. Ding, S. Wang, B.-J.J. Yao, W.-X.X. Wu, J.-L.L. Kan, Y. Liu, J. Wu, Y.-B. Bin Dong, Covalent organic framework based multifunctional self-sanitizing face masks, *J. Mater. Chem. A* 10 (2022) 3346–3358.
- [31] P. Das, G. Chakraborty, J. Roeser, S. Vogl, J. Rabeah, A. Thomas, Integrating bifunctionality and chemical stability in covalent organic frameworks via one-pot multicomponent reactions for solar-driven H₂O₂ production, *J. Am. Chem. Soc.* 145 (2023) 2975–2984.
- [32] Y. Li, M. Liu, J. Wu, J. Li, X. Yu, Q. Zhang, Highly stable β -ketoenamine-based covalent organic frameworks (COFs): synthesis and optoelectrical applications, *Front. Optoelectron* 15 (2022) 1–42.
- [33] J. Zhang, Y. Cao, W. Liu, T. Cao, J. Qian, J. Wang, X. Yao, A. Iqbal, W. Qin, Structural engineering of covalent organic frameworks comprising two electron acceptors improves photocatalytic performance, *ChemSusChem* 15 (2022) e202101510.
- [34] R. Gomes, A. Bhaumik, A new triazine functionalized luminescent covalent organic framework for nitroaromatic sensing and CO₂ storage, *RSC Adv.* 6 (2016) 28047–28054.
- [35] X. Miao, F. Zhang, Y. Wang, X. Dong, X. Lang, 2D β -ketoenamine-linked triazine covalent organic framework photocatalysis for selective oxidation of sulfides, *Sustain. Energy Fuels*. (2023).
- [36] X. Zhong, Q. Ling, Z. Ren, B. Hu, Immobilization of U(VI) onto covalent organic frameworks with the different periodic structure by photocatalytic reduction, *Appl. Catal. B Environ.* 326 (2023) 122398.
- [37] J. Liang, W. Li, J. Chen, X. Huang, Y. Liu, X. Zhang, W. Shu, B. Lei, H. Zhang, Carbon dots as an electron extractant for enhanced photocatalytic antibacterial activity of covalent organic frameworks, *J. Mater. Chem. A* 10 (2022) 23384–23394.
- [38] D. Kaleeswaran, P. Vishnoi, R. Murugavel, 3+3 Imine and β -ketoenamine tethered fluorescent covalent-organic frameworks for CO₂ uptake and nitroaromatic sensing, *J. Mater. Chem. C* 3 (2015) 7159–7171.
- [39] L. Yang, Y. Song, C. Lin, L. Hou, L. Guo, Y. Lei, L. Wang, Fluorescent core-shell SiO₂@vertical covalent organic frameworks nanosheets for sensing application, *Sens. Actuators B Chem.* 341 (2021) 129995.
- [40] S. Ghosh, T.S. Khan, A. Ghosh, A.H. Chowdhury, M.A. Haider, A. Khan, S.M. Islam, Utility of silver nanoparticles embedded covalent organic frameworks as recyclable catalysts for the sustainable synthesis of cyclic carbamates and 2-oxazolidinones via atmospheric cyclizative CO₂ capture, *ACS Sustain. Chem. Eng.* 8 (2020) 5495–5513.
- [41] R. Bywalez, H. Karacuban, H. Nienhaus, C. Schulz, H. Wiggers, Stabilization of mid-sized silicon nanoparticles by functionalization with acrylic acid, *Nanoscale Res. Lett.* 7 (1) (2012) 7.
- [42] X. Han, F. Zhao, Q. Shang, J. Zhao, X. Zhong, J. Zhang, Effect of nitrogen atom introduction on the photocatalytic hydrogen evolution activity of covalent triazine frameworks: experimental and theoretical study, *ChemSusChem* 15 (2022) e202200828.
- [43] G. Xia, J. Qiu, D. Dai, L. Zhang, Y. Tang, J. Yao, C. Jianhao Qiu, J. Co-, Electron-deficient covalent organic frameworks anchored on melamine sponges for visible-light-driven H₂O₂ evolution, *AIChE J.* (2023) e18192.
- [44] S.K. Das, B. Krishna Chandra, R.A. Molla, M. Sengupta, S.M. Islam, A. Majee, A. Bhaumik, CuO grafted triazine functionalized covalent organic framework as an efficient catalyst for C-C homo coupling reaction, *Mol. Catal.* 480 (2020) 110650.
- [45] N.A. Khan, R. Zhang, X. Wang, L. Cao, C.S. Azad, C. Fan, J. Yuan, M. Long, H. Wu, M.A. Olson, Z. Jiang, Assembling covalent organic framework membranes via phase switching for ultrafast molecular transport, *Nat. Commun.* 131 (13) (2022) 1–8.
- [46] H. Zhang, Z. Lin, P. Kidkhunthod, J. Guo, H. Zhang, H. Zhang, Z. Lin, J. Guo, Stable immobilization of nickel ions on covalent organic frameworks for panchromatic photocatalytic hydrogen evolution, *Angew. Chem. Int. Ed.* (2023) e202217527.
- [47] A. Basak, S. Karak, R. Banerjee, Covalent organic frameworks as porous pigments for photocatalytic metal-free C-H borylation, *J. Am. Chem. Soc.* (2023).
- [48] S. Zhong, Y. Wang, S. Li, S. Wang, X. Que, L. Sheng, J. Peng, L. Zhao, L. Yuan, M. Zhai, Enhanced photo-reduction of chromium(VI) from aqueous solution by nanosheet hybrids of covalent organic framework and graphene-phase carbon nitride, *Sep. Purif. Technol.* 294 (2022) 121204.
- [49] W.Y. Geng, X.X. Lu, H. Zhang, Y.H. Luo, Z.X. Wang, S.F. Guo, Z.Y. Zhou, D. E. Zhang, Effective design and synthesis of donor-acceptor covalent triazine polymers with boosted photocatalytic performance for Cr(VI) reduction, *Sep. Purif. Technol.* 290 (2022) 120829.
- [50] S. Ghosh, A. Nakada, M.A. Springer, T. Kawaguchi, K. Suzuki, H. Kaji, I. Baburin, A. Kuc, T. Heine, H. Suzuki, R. Abe, S. Seki, Identification of prime factors to maximize the photocatalytic hydrogen evolution of covalent organic frameworks, *J. Am. Chem. Soc.* 142 (2020) 9752–9762.
- [51] J. Dong, Y. Wang, G. Liu, Y. Cheng, D. Zhao, Isorecticular covalent organic frameworks for hydrocarbon uptake and separation: the important role of monomer planarity, *CrystEngComm* 19 (2017) 4899–4904.
- [52] G. Zhao, Y. Sun, Y. Yang, C. Zhang, Q. An, H. Guo, Molecular engineering regulation redox-dual-active-center covalent organic frameworks-based anode for high-performance Li storage, *EcoMat* 4 (2022) e12221.
- [53] Z. Sun, B. Liu, M. Li, C. Li, S. Zheng, Carboxyl-rich carbon nanocomposite based on natural diatomite as adsorbent for efficient removal of Cr (VI), *J. Mater. Res. Technol.* 9 (2020) 948–959.
- [54] Z. Shi, Z. Chen, Y. Zhang, X. Wang, T. Lu, Q. Wang, Z. Zhan, P. Zhang, COF TzDa/Ag/AgBr Z-scheme heterojunction photocatalyst for efficient visible light driven elimination of antibiotics tetracycline and heavy metal ion Cr(VI), *Sep. Purif. Technol.* 288 (2022) 120717.
- [55] N. Khosroshahi, M. Darabi Goudarzi, V. Safarifar, Fabrication of a novel heteroepitaxial structure from an MOF-on-MOF architecture as a photocatalyst for highly efficient Cr(VI) reduction, *New J. Chem.* 46 (2022) 3106–3115.
- [56] H. Arslanoglu, H.S. Altundogan, F. Tümen, Photocatalytic reduction of Cr(VI) from aqueous solutions with formic acid in the presence of bauxite: kinetics and mechanism, *Trans. Indian Inst. Met.* 74 (2021) 3075–3084.
- [57] H. Peng, J. Guo, Reduction behavior of chromium(VI) with oxalic acid in aqueous solution, *Sci. Rep.* 101 (10) (2020) 1–8.
- [58] Z. Wang, J. Yang, Y. Li, Q. Zhuang, J. Gu, Simultaneous degradation and removal of Cr(VI) from aqueous solution with Zr-based metal-organic frameworks bearing inherent reductive sites, *Chem. Eur. J.* 23 (2017) 15415–15423.
- [59] Z.C. Guo, M.L. You, Z.J. Wang, Z.F. Li, G. Li, Metal@COFs possess high proton conductivity with mixed conducting mechanisms, *ACS Appl. Mater. Interfaces* 14 (2022) 15687–15696.
- [60] J. Mao, L. Wang, S. Qu, Y. Zhang, J. Huang, H. She, Y. Bai, Q. Wang, Defect engineering in CuS x/COF hybridized heterostructures: synergistic facilitation of the charge migration for an efficacious photocatalytic conversion of CO₂ into CO, *Inorg. Chem.* 61 (2022) 20064–20072.
- [61] F. Zhang, Y. Zhang, G. Zhang, Z. Yang, D.D. Dionysiou, A. Zhu, Exceptional synergistic enhancement of the photocatalytic activity of SnS₂ by coupling with polyaniline and N-doped reduced graphene oxide, *Appl. Catal. B Environ.* 236 (2018) 53–63.
- [62] F. Zhao, Y. Liu, S. Ben Hammouda, B. Doshi, N. Guijarro, X. Min, C.J. Tang, M. Sillanpää, K. Sivula, S. Wang, MIL-101(Fe)/g-C₃N₄ for enhanced visible-light-driven photocatalysis toward simultaneous reduction of Cr(VI) and oxidation of bisphenol A in aqueous media, *Appl. Catal. B Environ.* 272 (2020) 119033.
- [63] Y. Luo, Y. Lan, X. Liu, M. Xue, L. Zhang, Z. Yin, X. He, X. Li, J. Yang, Z. Hong, M. Naushad, B. Gao, Hydrochar effectively removes aqueous Cr(VI) through synergistic adsorption and photoreduction, *Sep. Purif. Technol.* 317 (2023) 123926.
- [64] F. Zhang, X. Li, X. Dong, H. Hao, X. Lang, Thiazolo[5,4-d]thiazole-based covalent organic framework microspheres for blue light photocatalytic selective oxidation of amines with O₂, *Chin. J. Catal.* 43 (2022) 2395–2404.
- [65] Y. Wang, F. Huang, W. Sheng, X. Miao, X. Li, X.K. Gu, X. Lang, Blue light photocatalytic oxidation of sulfides to sulfoxides with oxygen over a thiazole-linked 2D covalent organic framework, *Appl. Catal. B Environ.* 338 (2023) 123070.
- [66] X. Chen, Y. Zhang, D. Yuan, W. Huang, J. Ding, H. Wan, W.L. Dai, G. Guan, One step method of structure engineering porous graphitic carbon nitride for efficient visible-light photocatalytic reduction of Cr(VI), *J. Mater. Sci. Technol.* 71 (2021) 211–220.
- [67] N. Luo, C. Chen, D. Yang, W. Hu, F. Dong, S defect-rich ultrathin 2D MoS₂: the role of S point-defects and S stripping-defects in the removal of Cr(VI) via synergistic adsorption and photocatalysis, *Appl. Catal. B Environ.* 299 (2021) 120664.
- [68] H. Zhang, L. Zhang, S. Dong, X. Duan, B. J. Ni, C. Lyu, Regulating energy band structures of triazine covalent organic frameworks with electron-donating/

- withdrawing substituents for visible-light-responsive photocatalytic tetracycline degradation and Cr(VI) reduction, *J. Hazard. Mater.* 446 (2023) 130756.
- [69] P.I. Uma, U.S. Shenoy, D.K. Bhat, Electronic structure engineering of BaTiO₃ cuboctahedrons by doping copper to enhance the photocatalytic activity for environmental remediation, *J. Alloy. Compd.* 948 (2023) 169600.
- [70] D. Xu, Y. Huang, Q. Ma, J. Qiao, X. Guo, Y. Wu, A 3D porous structured cellulose nanofibrils-based hydrogel with carbon dots-enhanced synergetic effects of adsorption and photocatalysis for effective Cr(VI) removal, *Chem. Eng. J.* 456 (2023) 141104.
- [71] M.E. Román Abarca, T. Kar, M. Casales-Díaz, J.J. Ramos-Hernández, S. Godavarthi, N. Pineda-Aguilar, V. Contreras, M. Calixto-Rodríguez, M.K. Kesarla, ZIF-8 derived carbon/g-C₃N₄ – an all-carbon heterojunction for effective photo-decontamination of Cr(VI) from water, *J. Alloy. Compd.* 960 (2023) 170623.
- [72] Z. Yong, T. Ma, Solar-to-H₂O₂ catalyzed by covalent organic frameworks, *Angew. Chem.* (2023), 2023) e202308980.
- [73] R. Kulkarni, Y. Noda, D. Kumar Barange, Y.S. Kochergin, P. Lyu, B. Balcarova, P. Nachtigall, M.J. Bojdys, Real-time optical and electronic sensing with a β -amino enone linked, triazine-containing 2D covalent organic framework, *Nat. Commun.* 101 (10) (2019) 1–8, 2019.
- [74] A. Bhati, S.R. Anand, D. Saini, S.K. Gunture, Sonkar, Sunlight-induced photoreduction of Cr(VI) to Cr(III) in wastewater by nitrogen-phosphorus-doped carbon dots, *Npj Clean. Water* 21 (2) (2019) 1–9, 2019.